Surface-Modified Photocatalysts

Claudio Minero

Abstract The surface properties of TiO_2 play a very important role in determining photocatalytic reaction efficiencies because heterogeneous photocatalytic reactions take place on the surface. Various parameters such as composition, phase structures, surface hydroxyl group, particle size, crystallinity, surface defects, and adsorbates or surface complexes play a key role. TiO_2 surfaces have been actively modified through manipulating the above parameters to enhance the photocatalytic performance. Here the main effects that influence the surface electron transfer are reported.

Keywords Adsorption of anions, Electron traps, Fluorides, Glycerol, Interfacial electron transfer

Contents

1 Introduction
2 Charge Carrier Trapping
  2.1 Electron Transfer Across the Interface
  2.2 Electron Transfer at the Interface
3 Change of TiO_2 Surface Speciation
  3.1 Adsorption of Cations
  3.2 Adsorption of Anions
4 Conclusions
References

C. Minero (✉)
Dipartimento di Chimica, Università di Torino, via Pietro Giuria 5, 10125 Torino, Italy
e-mail: claudio.minero@unito.it

D. Bahnemann and P. Robertson (eds.), *Environmental Photochemistry Part III*,
Hdb Env Chem, DOI 10.1007/698_2013_250,

1 Introduction

After photon absorption, charge carriers are generated. The high dielectric constant of TiO_2 assists in their separation, as charges become screened from their counter charges by the lattice. Charge separation follows energetic restrictions, and electrons/holes spatially migrate where a negative change of their free energy is allowed. Hot electrons and deep holes are more likely to separate than charge carriers generated with near-bandgap energy light [1]. Conversely, higher temperatures can negate the charge separation effectiveness [2]. An imposed electric field can assist in charge separation, just as a space charge region can [3].

Surface modification by extraneous phases as noble metal (platinum, silver, gold, palladium, and rhodium), copper, nickel, and oxide-on-oxide heterojunctions and also with other semiconductor will not be treated. All of these modifications are intended to favor charge separation and in addition can offer the potential for new reaction sites at the interface. The focus will be instead on naked surfaces and on the effect that the composition of the second phase at the interface has on the first.

The movement of charge carriers in spatial regions where the system gains free energy (minimum of their electrochemical potential) is called trapping. The interface or a bulk charge trapping site can separate one carrier from the other. Trapping could be considered beneficial if it is localized at the surface or if it promotes charge carrier separation. Conversely, trapping could be considered detrimental if trap sites are far from the site of electron transfer or lead to recombination. Trapping energies, if too large, could diminish the oxidizing potential of holes or the reducing potential of electrons, or inhibit rapid transport. If the trapping energy is small, any benefits of trapping would disappear. Then charge carrier could recombine transforming photon absorption energy in other photons or heat, less stored energy is available to the redox photocatalysis or for generating chemical fuels, and the rate of the overall process is slowed down.

The energies of surface electron trap states can be affected by applied potential (in an electrochemical system) [4], by local structure, by the deep-stabilizing self-polarization potential well induced by the air- or water-semiconductor dielectric mismatch, which is a function of the pore size and the bulk parameters of the matrix material [5], or by the presence of adsorbates. The trapping event likely involves structural relaxation that contributes to localization.

2 Charge Carrier Trapping

Electron traps are believed to be localized in the TiO_2 lattice as Ti^{3+} sites. TiO_2 surfaces in some cases act as charge trapping agents [6], depending on the spatial energy-band distribution. The transient absorption of nanocrystalline TiO_2 films in the visible (450–800 nm) and IR (2,500 nm) wavelength regions showed that surface-trapped electrons and surface-trapped holes were generated within 200 fs.

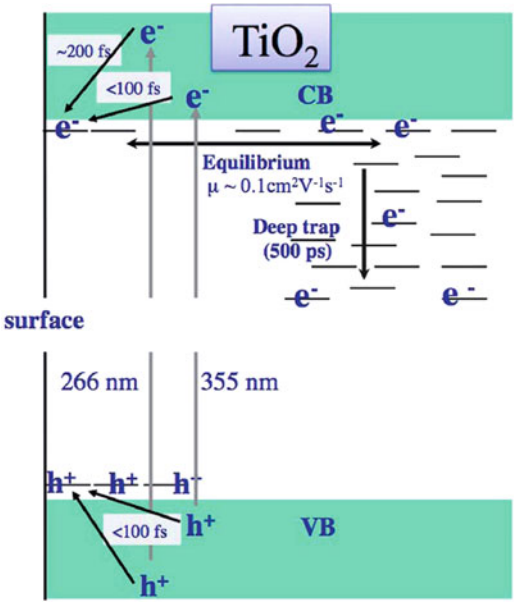

Fig. 1 The trapping and relaxation dynamics of electrons and holes in TiO_2 excited at 266 and 355 nm (from [9] with permission)

Surface-trapped electrons, which gave an absorption peak at around 800 nm, and bulk electrons, which absorbed in the IR wavelength region, decayed with a 500-ps time constant due to relaxation into deep bulk trapping sites. It is already known that, after this relaxation, electrons and holes survive for microseconds.

The electron trapping competes well with e−/h+ pair recombination even in the absence of a suitable hole scavenger [7]. The rate constant of electron-hole recombination in the bulk of a rutile TiO_2 single crystal was estimated to be $k_{rec} = 5 \times 10^{-13}$ cm^{-3} s^{-1} through sub-nanosecond time-resolved transient absorption spectroscopy. This value is more than four orders of magnitude smaller than the diffusion-limited rate constant ($k_{rec}^{diff} = 1.4 \times 10^{-8}$ cm^{-3} s^{-1}) for a rutile TiO_2 crystal, suggesting low recombination reactivity between electrons and holes in the crystal (Fig. 1) [8, 9].

There is a general agreement that electrons prefer trapping at the surfaces of TiO_2 [10–13] on defective sites just below the conduction band edge of TiO_2 in ranges of 0–0.35 V for anatase and 0–0.25 V for rutile [14]. On a chemical basis the most stable electron trap sites should be undercoordinated Ti cation sites located at surfaces. Based on Fourier transform infrared (FTIR) analysis [12, 15] photoexcited electrons are preferentially trapped at surface Ti-OH groups. A good examination of electron trapping is reported by the recent review of Henderson [16]. The electron trapping energy could range between 0.1 and 1 eV [14, 17], in agreement with photoemission results for electronic defects on the surface of TiO_2 single crystal surfaces [18].

While the trapping timescales are very short, the trapping lifetimes can be very long, particularly in the absence of electron scavengers such as O_2. Ethanol was

used as a hole scavenger to study electron trapping in synthesized nanocrystalline TiO_2 films and in films of commercial TiO_2 with transient absorption spectroscopy [13]. In the absence of ethanol and O_2, the transient signal at 800 nm (associated with excitation of trapped electrons) had a long half-life (~25 μs), suggesting a slow e^-/h^+ pair recombination at trap sites. In the presence of ethanol and the absence of O_2, electron trapping lifetimes were even longer (~0.5 s). These observations highlight the ability of TiO_2 surfaces to rapidly stabilize CB electrons in trap sites.

Hole trapping at rutile and anatase surfaces was also deeply explored [6, 19–26] particularly by means of hole scavenging chemicals such as SCN^-, organics, and I^-. In the absence of any hole scavengers at least two different types of traps have to be considered: (1) deeply trapped holes, rather long-lived and unreactive toward DCA^- nor to SCN^- ions, and (2) shallowly trapped holes that are at a thermally activated equilibrium with free holes and exhibit a very high oxidation potential [10]. EPR results indicate that the most likely hole trap site is a surface Ti^{4+}–O– site, where the hole resides on an undercoordinated surface oxygen atom, for which it is still uncertain what is its coordination (e.g., bridged or oxo type).

If the excited electron is removed with an electron scavenger, lifetimes for holes trapped at TiO_2 surfaces in the absence of hole scavengers have been estimated on the order of milliseconds to minutes [6, 27]. Hole trapping on the surfaces of TiO_2 appears to occur rapidly (~50 fs), as does electron trapping.

In the absence of an electron scavenger, electron trapping competes well with surface recombination when the number of e^-/h^+ pairs per particle is ~1, but the recombination is greatly favored as their number increases [7, 20]. The presence of a scavenger decreases the amount of recombination, which usually follows a second-order kinetics as required also by early kinetic models developed to explain chemical kinetics [28] and later validated [29]. The recombination rate depends on the surface-to-volume ratio of particles [30] because the bulk density influences absorptivity and the surface influences recombination. Several studies have explored the relationship between surface-trapped charges and charge recombination. For example, it was observed using EPR under bandgap irradiation of P25 that the majority of recombination events in P25 occurred at the surface or at the interfaces between particles or phases [23]. The analysis of the cyclic voltammetry response on thin rutile films revealed a strong dependence of the trap state concentration on the morphological structure. On the basis of results concerning the surface modification of the electrodes, these bandgap states where located at grain boundaries [31].

The trapped holes (and electrons) are less reactive than their bulk photogenerated precursors, although reaction of free carriers with surface chemisorbed molecules can be very rapid and efficient [10]. If charge recombination is governed predominately by the catalyst surface and its inherent structural heterogeneity, the texture and composition of the photocatalyst surface is of paramount importance.

Different TiO_2 specimens have a great chance to have different surface texture and composition and thus different probability that recombination events occur at the surface. The published data on particles morphology suggest a good uniformity of the Merck TiO_2 particle surfaces and a more defective surface for the P25

particles. In a recent paper [32] we reported by a comparative FTIR analysis under various conditions the presence of a variety of surface OH on P25, that is, at least 3 types of linear hydroxyl groups (in which OH is bound to a surface Ti, let's say Ti-OH) and 3 types of bridged hydroxyl groups (Ti-OH-Ti). There is a large consensus on the action of surface hydroxyls as surface hole traps, so their chemical nature is relevant to photocatalysis.

2.1 Electron Transfer Across the Interface

The electron transfer across the interface is at the heart of redox photocatalysis. Electron transfer is an interfacial phenomenon between a surface-trapped charge carrier and a chemisorbed or physisorbed species. In this session the electron transfer across the interface refers to the reaction of trapped species with solution or physisorbed species only.

In aqueous solutions metal oxides have pH-dependent surface charge which can be explained by the existence of acid/base equilibria. From infrared studies of the TiO_2-gas interface, it is known that the surface is hydroxylated when exposed to water vapor, with several types of hydroxyl species present. It has been suggested [33] that there is one chemically active face (001 on anatase and 110 on rutile) which contains both terminal and bridging OH groups. The other major crystal faces contain metal ions which are believed to only weakly bind water molecules. As already pointed out, depending on the specimen, different types of terminal and bridging OH groups could be present on TiO_2 [32].

Detailed studies on surface oxygen species on TiO_2 in a pH range 2.3–11.7 by internal reflection FTIR spectroscopy reported that Ti-OH is present in a pH range from 4.3 to 10.7 (maximum =8), Ti-OH_2^+ exists in a pH range below 5, and Ti-OH^+-Ti exists in a pH range below 4.3 [34]. There is also evidence for a surface water species which has an increasing population with increasing positive charge. At high pH the surface will be deprotonated with a negative charge. At some intermediate pH, the surface has net zero charge, and this pH is called the point of zero charge (PZC). A surface metal ion may have a residual charge which depends on the surface group and the crystal face. For a general review of the charge distribution, surface hydration, and the structure of the interface of metal hydroxides, see a recent review [35].

Application of the revised MUSIC model [36] to the vacuum-terminated rutile (110) surface was able to predict the formation and protonation of three unique types of surface oxygens upon surface hydration: (1) oxygen atoms in the Ti surface plane bonded to three Ti atoms that do not protonate in the accessible pH range (ca. 0–14); (2) bridging oxygens protruding above the Ti surface plane and bound to two surface Ti atoms that undergo a single protonation step in this pH range; (3) bare Ti atoms exposed at the surface that chemisorb a single water molecule, which may dissociate to form a hydroxyl group at sufficiently high pH. Bridging

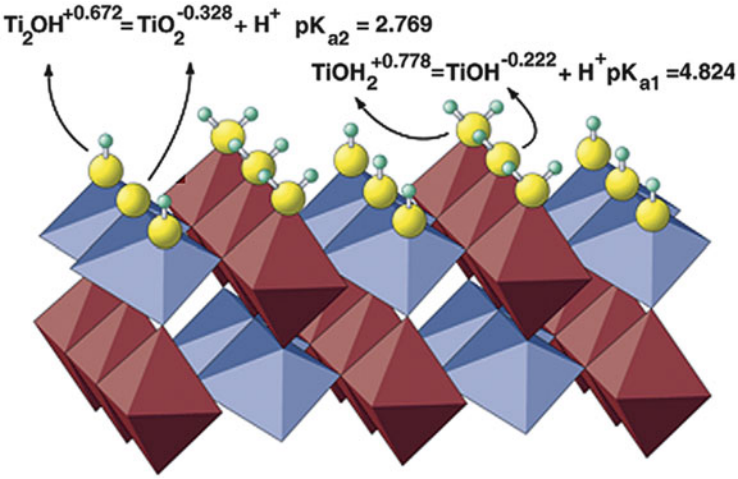

Fig. 2 Predicted protonation of hydrated (110) rutile surface by optimized MUSIC model. Protonation (*green spheres*) of surface oxygens (*yellow spheres*) reflects the four possible protonation states predicted by the revised MUSIC model: surface oxygens bridging two Ti octahedra (*blue* TiO_6 units) coordinate to one or zero protons, and surface oxygens at the apex of one Ti octahedral unit (*red* TiO_6 units) coordinate to one or two protons. The partial charges and equilibrium constants (pKa) were calculated with the MUSIC model using surface oxygen–Ti bond lengths predicted by ab initio calculations (from [37], with permission)

(Ti_2O and Ti_2OH) and terminal (Ti-OH and Ti-OH_2) protolytic surface oxygens are highlighted in Fig. 2 [37].

The effect of pH is also correlated to the anatase or rutile phase present and to their ratio [38]. In phenol decomposition the photocatalytic performance gradually and significantly increases with the anatase content. Photocatalysts containing only anatase as crystalline phase were up to three times more efficient than rutile ones. In salicylic acid decomposition, rutile-only catalysts were found to show no activity at all, but some of the prepared catalysts (both anatase-only and rutile-anatase mixtures) at pH 3 (but not at pH 7) displayed photocatalytic activity commensurable to that of Degussa P25.

In general pH variation changes the electrostatic interactions between the pH-dependent charge of the TiO_2 surface and the substrate. It is then apparent that the rate for the degradation of anionic dyes Methyl Orange, p-aminoazobenzene, Congo Red, and Brilliant Yellow was high at pH 5.6, while for cationic dyes like Rhodamine-B and Methylene Blue the highest rate was obtained in the alkaline pH 8.0 [39]. These differences can be accounted for by the adsorption capacity of the substrate on the catalyst surface under different pH conditions (see [40] for nitrophenols, where surface coverage can be manipulated with pH).

The TiO_2 CB edge exhibits Nernstian dependence with pH, shifting by −64 mV/pH unit in the range of −8 to +23 pH [18, 41].

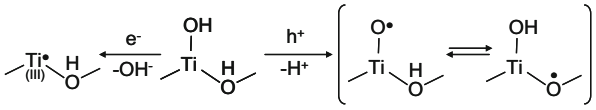

Fig. 3 Pictorial view of trapped electron and hole at the naked TiO_2 surface

From the pH dependence of transient absorption spectra in nanocrystalline TiO_2 films, two different trapped holes in the transient absorption spectrum have been identified. From their absorption spectra previously reported, spectra can be reproduced by their superposition [26]. In addition, they are significantly different from the expected shape of free carriers. This indicates that the holes in TiO_2 are trapped and that the spectral shape of holes reflects the condition of the trap states.

A very schematic and pictorial view of the trapped electron and hole at the naked TiO_2 surface is given in Fig. 3. As three types of linear hydroxyl groups and three types of bridged hydroxyl groups have been detected [32] on P25, the notation Ti(OH)(OH) refers to all of them. The species Ti(OH)(OH) can be protonated/deprotonated at various extent depending on solution pH.

The species in Fig. 3 at right are referred as (Ti(OH)(OH)) → (Ti(O•)(OH)) ⇆ (Ti(OH)(O•)), where the first (OH) refers to linear hydroxyl groups and the left (OH) to bridged hydroxyl groups. A shallow surface hole trap can be schematized as in the right of Fig. 3 where two limiting forms exist. The actual hole localization is formally regulated by their ratio K = [right]/[left]. The actual electron density distribution of the left and right forms in parenthesis are $1/(1+K)$ and $K/(1+K)$, respectively. The surface is considered hydrated to avoid to explicitly write charges that depend on the type of crystal face, the type of bridging oxygen, and the possible protonation and electron density [42]. The hole is stabilized at the surface by the surface hydration energy involved in the process $(TiO)_s + H_2O \rightarrow$ Ti(OH)(OH) and the pH-dependent release of protons that have a large hydration energy.

The schematic Ti(OH)(OH) for the (TiO_2) unit at the surface resumes many of the possible surface forms that a trapped hole (or electron) could have. In particular, in the framework of water oxidation, several other forms have been proposed, like $[Ti_2 = O\text{-}Ti]_s$ and $[Ti\text{-}O\text{-}Ti]_s$ that refer to a triply coordinated (normal) O atom and a bridging O atom at the surface, respectively [43]. For the trapped hole, the form $[Ti\text{-}O^{\bullet}\ HO\text{-}Ti]_s$ was also proposed, which is formed by a concerted hole and nucleophilic H_2O attack to $[Ti\text{-}O\text{-}Ti]_s$. This approach includes the possibility that surface oxygens are included in oxidation products and is consistent with surface reconstruction events and the phenomenon of superhydrophilicity [41]. The schematic of Fig. 3 loses this possibility and it is useful only for a general discussion of the electron transfer process. The resonance form of the trapped hole depicted inside parenthesis at left was supposed to be present only at pH > 13 [43]. According to the given picture, as Ti(O•)(OH) is not favored at acidic pH, and because the dissociation of the bridged hydroxyl occurring at pH > 8 with creation of a net negative charge on the bridged oxygen will further favor hole trapping on the oxygen, K will be >1 for naked titania and the most probable hole localization is Ti(OH)(O•), i.e., on bridged oxygen.

This also outlines the role of solution pH on the electron transfer rate. As the surface at acidic pH is positively charged, the electron abstraction from $Ti(OH_2^+)(OH)$ is more difficult, implying that the hole trap $Ti(OH_2^+)(O\bullet)$ is shallower that $Ti(OH)(O\bullet)$. From this it follows a greater potential difference with the redox potential of the substrate to be oxidized and a greater reaction rate. At basic pH the $Ti(O^-)(O\bullet)$ is stabilized, as an electron is easily abstracted from a negative surface. This implies a lower oxidizing potential and reduced trapped hole reactivity. Conversely the electron trapping at Fig. 3 (left) is favored by acidic pH, forming a trap with reduced reducing potential. This will limit reactivity toward physisorbed oxidants. This picture is in agreement with experimental results obtained by transient techniques. Tracking Methyl Orange photodecomposition on suspended P25 as a function of pH, a crossover at pH ~8 was detected between an oxidative and a reductive pathway for degradation [44]. Above a pH of 8, the rate-limiting step was oxidation and O_2 reduction was rate limiting at lower pH values. The reducing species becomes more reactive at higher pH, the converse being valid for the oxidizing carrier, as a result of the shift in electrical potential of TiO_2 particles. This conclusion accords also with recent results obtained using highly ordered TiO_2 nanotube prepared by an anodic oxidation method. It was found that 2,3-dichlophenol in alkaline solution was degraded and dechlorinated (a reductive process) faster than that in acidic solution, whereas dissolved organic carbon removal presented an opposite order in dependence of pH [45].

The pH can be varied to shift band positions and surface electrostatics that influence charge carrier dynamics as discussed above [44] and photoluminescence [43]. The shifts in band edges induced by changing pH can be used to control some electron transfer process or possibly shift conditions from oxidative to reductive [44]. The effect of pH is important for practical application. In the removal of cations from solution, the system pH controls the speciation in solution and the interfacial electron transfer. The photocatalytic removal of Hg(II) from aqueous solutions of $HgCl_2$ using TiO_2 as catalyst showed that the overall process strongly depended on pH, being enhanced as the pH was increased [46]. At pH 10, an efficient removal of Hg(II) was achieved even in the absence of organic additives, attaining final mercury concentrations in solution at trace levels ($\mu g\ L^{-1}$). In acidic conditions, the addition of sacrificial organic molecules significantly increased the rate and extent of aqueous Hg(II) removal. The nature and distribution of mercury products deposited on the catalyst were dependent on the reaction conditions. Reported evidences showed that it cannot be established a direct correlation between Hg(II) dark adsorption on the TiO_2 surface and the efficiency of Hg (II) photoreduction achieved.

Electron and hole transfer plausibly occurs at spatially separated surface traps. It has been demonstrated on both rutile and anatase microcrystals that the reductive and oxidative processes take place on different crystallographic faces [47]. Reductive facets are (110) and (101); oxidative facets are (011) and (001) for rutile and anatase, respectively. It is reasonable to assume that these two processes are not competing for the same surface sites. The presence of distinct sites for oxygen reduction supports the possibility that under complete coverage by ligands (see below) the scavenging of electrons will still be possible.

Recombination will occur by free electrons in CB with holes that are trapped on titania with both tautomeric forms of Fig. 3.

On the reductive side, electron transfer to O_2 forms an O_2 molecularly adsorbed state. O_2 can only physisorb to TiO_2 surfaces if reduced cation sites are not present [48]. Some OH groups associated with electron trap sites are altered by O_2 exposure, but others are not [12]. The interaction of O_2 with bridging OH groups (OH_{br}) results in the extraction of charge and a proton from the OH_{br} groups [49]. Berger et al. [2] using EPR results and simulations attributed signals to reaction of O_2 with a trapped electron to form O_2^-. Bahnemann et al. [10] have shown that the relative rate of O_2^- formation from the reaction of O_2 with trapped electrons was roughly 100 times slower than for the reaction of O_2 with solvated electrons in solution and that this represents a major bottleneck for photooxidation reactions. The O_2^- species appeared to be the intermediate through which a variety of potentially important reactive oxygen-containing species, such as O_2^{2-} and H_2O_2/HO_2, were photochemically formed. The primary step of photocatalytic O_2 reduction is the formation of the surface peroxo species, $Ti(O_2)$, giving the 943 cm^{-1} band, probably with the surface peroxo species, $TiOO^{\bullet}$, as a precursor, in neutral and acidic solutions. The surface peroxo species is then transformed to the surface hydroperoxo, TiOOH, giving the 838 and 1,250–1,120 cm^{-1} bands, by protonation in the dark [50]. Spectroscopic observations of $HO_2^{\bullet}$ and production of H_2O_2 [51] have been linked to reactions of O_2 with water-related species on or near the TiO_2 surface. It is extensively conjectured that O_2 chemistry in the reductive side of photocatalytic systems results in hydroxyl radicals that can participate in oxidative reactions.

On the oxidative side, the electron transfer event across the interface is usually quite fast. For example, for an aqueous I^-, hole transfer occurs on less than 10 ns [7]. The amount of I_2^- (product of oxidation) was observed relatively stable during the first 4 μs, in contrast to the decay of the electron population due to recombination which is only slightly different than in iodide-free solutions.

Reaction of holes with organic (reduced) molecules could be direct (direct electron transfer from the substrate to the valence band hole) or mediated by OH radicals either free or bound. Examples of remote oxidation [52, 53] through gas phase have been reported. In this phenomenon, oxidation events occur at regions of a TiO_2 sample not exposed to light or at locations that are apart from irradiated TiO_2 surfaces. Although oxidizing species could be formed in the gas phase from O_2 by subsequent reduction, evidence supports the surface generation of OH radicals [54].

Reports on the presence of free OH in solution are conflicting. The ESR detection of OH radicals on irradiated TiO_2 (anatase) at 77 K was reported [55], although the ESR signals showed no spectral change by H_2O/D_2O exchange. Ultraviolet photoelectron spectroscopic studies combined with scanning tunneling microscopy revealed that the O_{2p} levels for bridging hydroxyls groups (Ti-OH-Ti) at the (110) face and terminal hydroxyls groups (Ti-OH) at the (100) face of rutile are both far below the top of the valence band [56] to oxidize water. These results are confirmed by theoretical calculations [57]. Nosaka et al. pointed out that the water photooxidation reaction at TiO_2 produced no free OH radical, and

spin-trapping agents reacted with surface-trapped holes (adsorbed OH radicals, see Fig. 3) [58]. Early ESR measurements showed that photogenerated holes were trapped at lattice O atoms (or Ti-O-Ti sites) at low temperatures of 4.2 or 77 K and did not produce OH radicals [59]. Micic et al. confirmed this conclusion and showed clearly that not OH radicals but surface-trapped radicals were involved in the methanol oxidation that proceeded by charge transfer from the oxygen lattice holes [60]. Serpone et al. reported a fast trapping in some adsorbed state of the OH radicals generated by pulse radiolysis onto the TiO_2 surface [61]. It is argued that the trapped hole and a surface-bound OH radical are indistinguishable species. Later studies showed that the reaction of TiO_2 with OH radicals probably does not form an adsorbed radical on the surface, but OH radicals inject holes into TiO_2 and subsequently form a charge transfer complexes between the holes and OH^- ions [26].

A direct convincing evidence that photogenerated species do not migrate far from the catalyst surface has been derived from the study of the degradation of decafluorobiphenyl (DFBP), a substrate that is strongly adsorbed (>99%) on alumina and TiO_2 [62]. When DFBP is adsorbed on alumina particles and mixed with titania particles, the amount exchanged is very low (<5%). Irradiation of DFBP adsorbed on alumina in the presence of H_2O_2 (generating OH in solution) or titania colloids (supposed to generate OH free or bound to the surface on mobile particles) leads to degradation, while DFBP is not degraded when larger titania particles (P25, TiO_2 beads) are present. Pentafluorophenol, which is easily exchanged between the two oxides, is photodegraded in all cases. This makes clear that active species formed upon irradiation do not migrate in solution, while the organic substrate may or not migrate to the catalyst surface. Only when both are present at the catalyst surface the degradation takes place.

For a poorly adsorbed substrate like phenol [63], the detailed kinetic analysis and the time evolution of the intermediates in the presence of different alcohols (tert-butyl alcohol, 2-propanol, and furfuryl alcohol used as hydroxyl radical scavengers) suggested that the oxidation of phenol proceeds for 90% through the reaction with surface-bound hydroxyl radical (Ti(OH)(O•), the remaining 10% via a direct interaction with the VB holes [64].

2.2 Electron Transfer at the Interface

If species are chemisorbed, it is trivial that the physical and electronic structures of the adsorbed state of the molecule have been changed. How a molecule binds on the TiO_2 surface influences its electronic structure and redox properties. There are many reports dealing with the thermodynamic of adsorption on the TiO_2 surface. The review by Thornton et al. [65] reports many of these cases, in particular the cases of HCOOH and C2–C8 alcohols.

The electronic structure and redox properties of undercoordinated Ti cations located at the surface, which likely act as more powerful adsorbing sites, will

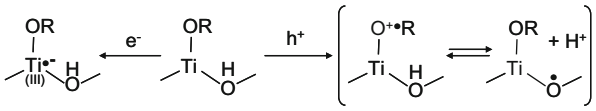

Fig. 4 Pictorial view of trapped electron and hole at an adsorption site

change with adsorption, *changing the energetic properties of electron traps* and the related charge carrier dynamics. The same holds for hole traps, as localization of the surface hole on bridged oxygen is influenced by near complexed titanium cations.

A very schematic and pictorial view of trapped electron and hole at the adsorption site on the TiO_2 surface, with limits already discussed for Fig. 3, is given in Fig. 4. The electron transfer at the interface implies the reaction of the charge carrier with adsorbed species giving a trapped charge carrier. Under this assumption an inner sphere electron transfer is implicated. The energy of the trap (trapped charge carrier) depends on adsorption (or complexing) free energy of the adsorbate. For the electrochemical half reaction depicted at right of Fig. 4, according to the Nernst law, the energy of the trap depends on the ratio of the formation constants β_{ox} of the substrate with the oxidized Ti(OH)(O•)) site to give (Ti(OR^+ •)(OH)) ⇆ (Ti(OR)(O•)) and the formation constants β_{rid} of the substrate with the site Ti(OH)(OH)) to give the reduced surface complex Ti(OR)(OH)). If $\beta_{rid}/\beta_{ox} < 1$, then the oxidant potential of the trap is reduced, forming an intra-bandgap surface-trapped hole. As Ti(OR)(O•) is more stable than Ti(OH)(O•), which is always true when −OR replaces −OH, the Ti(OR)O•) trap is deeper than Ti(OH)(O•).

In the cited work of Rabani et al. [7], alcohols (methanol and 2-propanol) at high concentrations unexpectedly reduce the initially observed electron population by up to fourfold, without affecting the shape of the nanosecond time profile. The alcohol effect was assigned to the formation of an alcoholic-positive ion radical (free) which is more reactive in recombination with conduction band electrons than the original hole. This is in our opinion the first spectroscopic evidence of a substrate-mediated charge recombination that was supposed in macroscopic kinetic model (called back reaction) [28] to explain the peaked dependence of the rate from the substrate concentration.

More recently by highly sensitive femtosecond and nanosecond spectroscopy under low-intensity excitation conditions to avoid fast electron-hole recombination, it was observed [27] that electron transfer from trapped holes in TiO_2 occurs over a wide timescale depending on the alcohol. The lifetimes of trapped holes in the films in methanol, ethanol, and 2-propanol are 0.3, 1.0, and 3.0 ns, respectively. The authors suggested that it is likely that the rate-limiting step in this experiment is hole transfer from trapping sites to alcohol molecules and that the oxidation reactions of alcohols can be regarded as electron transfer from alkoxy species to adjacent surface holes (unoccupied surface states just above the valence band), but concluded that the reason for the different oxidation times for different alcohols was unclear. According to the simplified picture given in Fig. 4, the hole transfer does not follow an outer sphere mechanism, but is an inner sphere electron transfer at the

surface complex. The different alcohols would give different hole traps, and the rate-limiting step is the release of products from (Ti(OR^+•)(OH)).

By comparing the photocurrent yields versus the extent of organic photooxidation on P25-covered anodes under anaerobic conditions, it emerged that the efficiency of hole acceptors in four adsorbed organics followed the trend: oxalate > formate > acetate > methanol [66]. This trend did not correlate with the relative reaction rates of these molecules with free OH• in solution, but is consistent with the trap energy that depends as discussed above from the formation constant of the surface complex. Recently it was demonstrated that the oxidation of oxalate proceeds on the surface of rutile nanowires mainly via the bridging bidentate bioxalate (large formation constant), followed by a fast replenishment of photooxidized species by monodentate bioxalate [67].

A different reactivity from that of free OH• in solution has been also seen changing the substrate concentration and consequently the amount of substrate adsorbed on the TiO_2 surface. The main reaction products obtained from glycerol on irradiated TiO_2 P25 depend on glycerol concentration [68]. At low concentration glyceraldehyde and dihydroxyacetone (C3 compounds) are formed in a relative ratio about 2, together with formaldehyde and glycolaldehyde. As the glycerol concentration increases and glycerol rate is strongly depressed, the main products are formaldehyde and glycolaldehyde. For Merck TiO_2 the main products of phototransformation are the two C3 carbohydrates with relative ratio ranging from 1.3 to 1.8, according to an •OH-related chemistry. The evident experimental result is that mainly the two C3 carbohydrates are produced from glycerol in the presence of fluorides that competitively adsorb on the surface (see also below). On Merck TiO_2 almost no change is observed with addition of fluorides, while on P25 the production of formaldehyde and glycolaldehyde was strongly depressed. As fluorides impede the surface complexation on the surface Ti-OH site, the formation of formaldehyde and glycolaldehyde is strictly connected with glycerol chemisorption.

All these findings (except the oxalate case for which hole transfer is followed by electron injection in CB) lead to the conclusion that when a chemical species is strongly bound to the surface, its overall degradation rate is generally different from that in the physisorbed state and could be depressed (see the case of catechol [63]). Although the strong binding to the surface favors reactions with holes, this implies that the species is more subject to back reactions with electrons, resulting in a decreased overall rate of oxidation. Furthermore, the two mechanisms, the electron transfer across the interface and the electron transfer at the interface, depend at a large extent on the adsorption of substrates and thus depend on the concentration of the substrate in the free phase or on the concurrent equilibria (acid/base, concurrent complexation) that influence its adsorption. So the literature results could be somehow confusing because the concentration effect is mistreated. To add some complication, often the net result of a primary step of a chemical reaction could be the result of both oxidative and reductive processes. For example, it was recently showed through isotopic-labeling examinations combined with DRIFTS and electrochemical experiments that, contrary to the radical Kolbe decarboxylation, the decarboxylation of saturated carboxylic acids is possible by a concerted

mechanism [69]. At first step, the pristine acid is oxidized to α-keto acid by holes or (adsorbed) OH radicals without loss of carbon atoms, and then, the intermediate α-keto acid is decarboxylated to shorter-chain acid through an e_{CB}/O_2 process, in which an oxygen atom of O_2 is selectively incorporated into product.

3 Change of TiO_2 Surface Speciation

A modification of the surface speciation would change the nature of surface traps and the overall charge carrier dynamics. As the pH effect and the complexing ability of the substrate on the hole trap energy have been already discussed, here two main additional categories of processes that change the state of the surface will be considered.

The anatase/water interface and, more generally, the metal/oxide water interface are characterized by a charge build-up whose entity and sign not only is pH dependent but also results from the specific adsorption of ions [70]. Various cations, anions, and neutral molecules were found to affect the rate of chloroform degradation. At pH 7 addition of 1 mM Co^{2+} decreased the reaction rate by more than 50%, 0.2 mM Al^{3+} reduced the rate by 70%, and 0.5 mM Zn^{2+} reduced the rate by 60%. The addition ClO_4^- did not affect the rate, F^- increased by 15%, and Cl^- and PO_4^{3-} decreased the rate depending on pH [71]. It is recognized that the flat-band potential of semiconductor oxides, and, consequently, the positions of the band edges, depends on the nature and composition of the electrolyte. Specific adsorption of ions can shift the flat-band position significantly. The adsorption of ions can thus change the driving force of electron transfer and introduce surface states that can act as carrier trapping sites and recombination centers and can inhibit the adsorption of other species.

3.1 Adsorption of Cations

Metal cations adsorbed on a TiO_2 surface can act as sites where electron transfer is enhanced/inhibited, as sites at which charge carriers are separated and/or trapped, and as sites where charges recombine. Metal cations could be incorporated in the TiO_2 lattice or segregated at the surface during a sol–gel or impregnation methods. Because such syntheses typically result in both surface and bulk modifications of TiO_2, it becomes difficult to distinguish between bulk and surface effects. Transition metal cations that have redox properties (Cu^+/Cu^{2+}, Fe^{3+}, V^{5+}, and Cr^{3+}) can act as electron acceptors from the TiO_2 CB, promoting charge carrier separation and efficient photooxidation [72]. Particularly in the case of gas/solid reactions, these deposited metals generate new catalytic sites. For example, isolated surface Cu^+ sites on TiO_2 promoted CO_2 photodissociation to CO [73], and surface Fe^{3+} cations enhanced maleic acid photooxidation [74]. Metal cations like Cu, V, or Cr loaded onto TiO_2 during the sol–gel procedure raised NO photooxidation because it

enhanced adsorption [75]. In some cases, the ability of adsorbed metal cations to scavenge CB electrons had a competitive effect on O_2 photoreduction, particularly when the reaction products of O_2 photoreduction were needed to promote indirect oxidation processes [76].

The metal cation adsorption could enhance the adsorption by altering the electrostatics at the surface that promote or inhibit electron transfer processes. When TiO_2 plays a passive role as in DSSC, the oxidation of I^- and formation of I_2^- were facilitated with alkali promoters (Mg^{2+}, Li^+, Na^+ and K^+) that can reverse the surface charge from negative to positive, stabilize I^- at the surface, and enhance its rate of oxidation by a photoionized dye [77].

Few examples are reported for adsorption from solutions. The metal cation adsorption on the surface of TiO_2 could *block/impede the adsorption* of the substrate redox species. This could limit the application of photocatalysis to high ionic strength media, like seawater [78]. However, adsorbed Al^{3+} cations halted poisoning caused by adsorption of strongly bound surface intermediates on TiO_2 during salicylic acid photodegradation [79]. In anatase/water systems under bandgap irradiation, both the organic substrate (formate) oxidation initiated by photogenerated valence band holes and the formation of hydrogen peroxide from O_2 reduction (by conduction band electrons) are strongly influenced by the presence of Zn^{2+} cations [80]. Depending on the pH, the formate oxidation rate can be enhanced or nearly completely inhibited. The observed result can be rationalized by considering the fraction of Ti-OH surface sites blocked by inner sphere complexation of Zn^{2+} as a function of pH. When this fraction is low, the more positive surface charge favors formate oxidation, whereas when the fraction is high, the almost complete blockage of Ti-OH surface sites by Zn^{2+} stops almost entirely formate oxidation.

3.2 Adsorption of Anions

The interest on the effect of anions (carbonate, chloride, sulfate, and nitrate) started from application to wastewater treatment. The surface occupation by anions may be competitive with adsorption of organic molecules. This effect is directly related to their coverage fraction. At the surface anions are subjected to redox transformations after electron transfer with photogenerated charge carriers (as for ClO_2^-, ClO_3^-, NO_2^-, and NO_3^- [30]). This second effect could produce inhibition by competition of inorganic ions with the organics. In a recent paper, the inhibition of photocatalytic degradation of 2,3-dichlophenol on highly ordered TiO_2 nanotube arrays prepared on titanium sheets was larger for $SO_4^{2-} > Cl^- > H_2PO_4^- > NO_3^-$. The observed inhibition effect was attributed to the competitive adsorption and the formation of less reactive radicals during the photocatalytic reaction [45]. For example, phosphate binds strongly to TiO_2, with a Langmuir binding constant at pH = 2.3 $K_{ads} = (3.8 \pm 0.8) \times 10^4\ dm^3\ mol^{-1}$, which is similar to the binding constants onto TiO_2 for bidentate ligand species such as oxalate and

catechol [81]. The adsorption strongly changes the water structure at titanium dioxide interface [82]. In the presence of Cl^- anions, the surface had an isoelectric point near pH 5.5 and showed the least degree of water organization near this pH. The phosphate ions shifted the isoelectric point of the interface to pH 2.0, and the intensity of the 3,400 cm^{-1} peak was significantly increased in comparison with the chlorides data at both neutral and acidic pH values. Flat-band potentials determined by Mott–Schottky analysis in the absence of phosphate were Nernstian only for pH 3–7. With the addition of phosphate, impedance spectroscopy results showed additional space charge capacitance, peaking at potentials 150 mV positive of the flat-band potential [70].

Then drastic changes are caused on reactivity by manipulation of the surface chemical composition via exchange of surface hydroxyl groups.

It is long known that fluoride adsorbs onto TiO_2 surfaces (see, e.g., [83]), and the adsorption of fluoride inhibits the adsorption of other ligands, e.g., catechol and hydrogen peroxide [51, 63]. Fluorination of P25 greatly simplifies the surface IR spectrum [32], leaving only the component at 3,674 cm^{-1} that was assigned to one type of bridged hydroxyl groups. The νOH components removed by fluorination can be ascribed to hydroxyls sitting on defective sites, which interact more strongly with ligands. The surface of TiO_2 P25 is characterized by the presence of at least two different hydroxyls, with different coordination strength toward fluorides (and presumably to other ligands). The confirmation of this picture comes from the evolution of νOH patterns for Merck TiO_2 and their comparison with P25. Pristine and fluorinated Merck TiO_2 show similar νOH pattern, with a dominant spectroscopic feature at 3,674 cm^{-1}. The effect of fluorination in this case is the decrease of the intensity at 3,674 cm^{-1}, but the pattern does not change. The spectra of pristine and fluorinated Merck TiO_2 are very similar to that of fluorinated P25. As demonstrated by Sun et al. [84], fluoride preferentially adsorb on the {001} facets. Surface Ti(VI) ions on these facets are more exposed, so more coordinatively unsaturated, with respect to the more stable {101} facets.

In general, the complexation between surface Ti(IV) sites and ligands should affect the surface charge density and consequently the zeta potentials. The zeta potentials of suspended TiO_2 particles in water as a function of pH and $[F^-]$ have been reported [85]. The PZC of TiO_2 is measured to be ca. pH 6.2, which is in agreement with the literature values. In the presence of F^-, the PZC is shifted to lower pH values, and the positive charge on TiO_2 surface at acidic pH region is much reduced since no more surface hydroxyls on Ti(F)(OH) are available to be protonated. As a result, the concentration of tetramethylammonium ion $(CH_3)_4N^+$) at the TiO_2/water interface at pH 3 was higher on F-TiO_2 than on naked TiO_2 film due to a reduced electrostatic repulsion between the cation and the surface [86].

Since the first reports in 2000 [63, 64], hundreds of papers have been published on this issue. Surface fluorination improves the photocatalytic degradation of a number of simple organic compounds, such as phenol [63], benzoic acid [87, 88], benzene [89], cyanide [90], and N-nitrosodimethylamine [91], and for a variety of organic dyes [92–96]. The positive effect on the photocatalytic degradation has been directly associated with the displacement of OH terminal groups from the

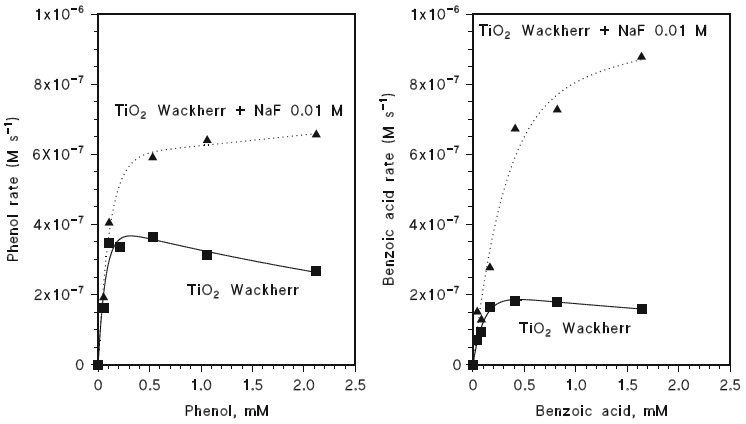

Fig. 5 Degradation rate of phenol and benzoic acid on Wackherr TiO_2 as a function of the substrate concentration in the absence and presence of fluoride ions at pH 3 (adapted from [87])

TiO_2 surface. The first hypothesis was that fluorination would enhance the generation of free OH radicals [63]. Acid Red 1 degradation mainly occurs via direct electron transfer because its rate is not depressed by 2-propanol addition on naked TiO_2. On the contrary, a strong decrease in the Acid Red 1 bleaching rate was observed upon 2-propanol addition on fluorinated TiO_2, indicating that oxidative paths through hydroxyl radicals play a major role under these conditions [97]. The convincing demonstration of the relevance of hydroxyl radicals on fluorinated TiO_2 was achieved by detecting the DMPO-OH adduct produced by irradiating unmodified and F-modified TiO2 suspensions [97]. As a consequence, the oxidation of the organic substrates would occur in solution, where the probability of back reaction (reduction) is reduced. Along the same line is the remote photocatalytic oxidation of stearic acids over the surface-fluorinated TiO_2 film monitored by Fourier transform infrared measurement and gas-chromatographic CO_2 production analysis, which was markedly faster with F-TiO_2 than with the pure TiO_2 film [98]. The production of CO_2 that evolved as a result of the remote oxidation of stearic acids was enhanced when H_2O_2 vapor was present but was strongly inhibited in the presence of ammonia gas that should scavenge OH radicals. These evidences suggested that the airborne oxidants in remote photocatalytic oxidation are most likely OH radicals and the surface fluorination of TiO_2 seems to facilitate desorption of OH radicals.

A comparison between the rate of degradation as a function of substrate concentration for phenol and benzoic acid shows that the effect of fluoride is more marked for benzoic acid than for phenol (see Fig. 5) [87]. Benzoic acid adsorbs on the surface of naked TiO_2 much more than phenol does. Interestingly the functional form of the rate is far from a Langmuir type and it is similar in the two cases, showing a decrement with increasing concentration. The rate of benzoic acid is lower than that of phenol and the reverse is seen in the presence of fluorides. This suggests that the adsorption is detrimental to the rate of degradation and that the

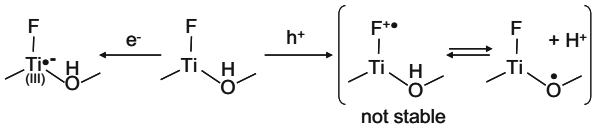

Fig. 6 Pictorial view of trapped electron and hole at the fluorinated TiO_2 surface

substrate surface complex can act as a recombination center (back reaction with CB electrons). This will be further discussed below using glycerol as substrate.

A decrease in photoactivity upon illumination was observed for formic acid [88] and dichloroacetate [85], species that are strongly bound to the TiO_2 surface. In the degradation of formic acid that adsorbs on the TiO_2 surface [51], it has been shown that no H_2O_2 is formed in the absence of (1) fluoride ions; (2) a hole scavenger; (3) oxygen, even in the presence of fluoride and Ag+ as electron scavenger. The surface fluorination of TiO_2 strongly promoted the photochemical production of hydrogen peroxide, the production rate of which was proportional to the surface Ti-F coverage. On the other hand, the degradation of H_2O_2 under photocatalytic conditions was inhibited by the presence of fluoride. Anions without surface complexing abilities (e.g., nitrate) did not lead to H_2O_2 formation. This suggests that the peroxides produced by O_2 reduction, when their adsorption is inhibited, are left in solution to be further reduced to H_2O_2, and when they are adsorbed, they act as recombination centers for holes. For all the above evidences [51, 85, 88], the explanation was that fluoride can displace peroxides from the Ti(IV) surface sites [99] hindering the direct hole transfer [100].

However, also the importance of fluorination on the electron transfer rate has been recognized [101]. By means of photopotential decay measurements, it was demonstrated that TiO_2 surface fluorination retards the reactivity of photogenerated electrons both for recombination with surface-trapped holes and for transfer to oxygen, upward shifts the electronic levels in the potential energy scale, changes the mechanism from direct to indirect for strong adsorbing species, and inhibits the adsorption of intermediates that could serve as recombination centers [102, 103].

A very schematic and pictorial view of trapped electron and hole at the adsorption site on the fluorinated TiO_2 surface, with limits already discussed for Fig. 3, is given in Fig. 6.

For fluorinated titania, some (but not all [32]) of the terminal hydroxyls are exchanged with fluoride, and the left tautomeric form is impeded by the high fluoride electronegativity. Thus $K/(1+K) \approx 1$ and $K >> 1$. In addition, as fluoride is more electronegative than −OH, the radical on bridging oxygen is less stable, i.e., the surface trap Ti(F)(O•) is more shallow than Ti(OH)(O•), and its energy level is more resonant with free holes in the valence band. This is consistent with the application to the half reaction at right of Fig. 6 of the Nernst law. The energy of the trap depends on the ratio of the formation constants β_{ox} of fluoride ion with the oxidized Ti(OH)(O•)) site to give (Ti(F)(O•)) and the formation constants β_{rid} of the fluoride ion with the site Ti(OH)(OH)) to give the reduced surface complex Ti(F)(OH)). As fluoride ions are able to displace from the surface most of organics, β_{rid} is

very large. Conversely, as the left resonant form in parenthesis is not stable, $\beta_{rid}/\beta_{ox} > 1$, and the oxidant potential of the trap is increased. Its *value could then be very close to the oxidant potential of the VB free hole*. Since fluorination increases the rate for substrates that react with OH radicals and depresses the rate for substrates that react by direct electron transfer, the right form *Ti(F)(O•) performs as an OH radical*. In recent reconsideration of surface fluorination [104], the decrease of the recombination rate concurrent with the increase of the electron transfer rate with reduced dissolved species is invoked to explain the fluoride effect.

Due to the different electron affinity of the groups involved, also free electrons are more stabilized on −Ti(F)− than on −Ti(OH)− and the surface-assisted recombination is reduced. No experimental evidence is reported on the stability of the $Ti^{\bullet -}$(F)(OH) species depicted at left of Fig. 6. A release in solution of F− would change this species to $Ti^{\bullet}$()(OH) as in Fig. 3 (left). However, the reduced rate of O_2 reduction on fluorinated TiO_2 with respect to the naked one [102, 103] suggests that chemisorption is not allowed and the possible electron trap is that depicted in Fig. 6.

Alcohols, polyols, and carboxylic acids show good coordinative abilities toward Ti(IV) ions. At suitable concentration, these species are able to occupy surface sites. Surface complexation will form a surface deep trap for holes, as the oxidation potential of the surface complex Ti(OR)(OH) is lowered with respect to Ti(OH)(OH). Besides being an efficient recombination center, the oxidized surface complex (Ti($^{+}$•OR)(OH)) is an alkoxy radical-like species that has a chemical reactivity very different from the carbon-centered radical •OR generated via H-abstraction by the surface adsorbed OH•, namely, the Ti(OH)(O•) hole trap [105]. This was demonstrated using glycerol as substrate.

In this case the two produced carbon-centered radicals evolve to dihydroxyacetone (C3) or glycerolaldehyde (C3), while the surface complex (Ti($^{+}$•OR)(OH)) undergoes β-scission, giving formaldehyde (C1) and a second carbon-centered radical, which by reaction with molecular oxygen at diffusion controlled rates produces glycolaldehyde (C2) and hydroperoxydes. The reported case is quite interesting because, as β-scission is a slow process, an inhibition of the reaction rate is observed when all the surface hydroxyls are exchanged with glycerol. The deep-trapped hole (Ti($^{+}$•OR)(OH)) must recombine free electrons more easily than (Ti(OH)(O•)). In fact numerical simulation of the rate dependence on glycerol concentration showed that the kinetic profile is correct only if the deep-trapped hole (Ti($^{+}$•OR)(OH)) has a very high kinetic constant for electron recombination. It is also worth noting that the shift of the mechanism from an oxidative attack to not chemisorbed glycerol mediated by Ti(OH)(O•) shallow surface hole traps, to a direct hole transfer to the surface complex, leads to very different intermediates.

In the presence of fluorides that competitively adsorb on the surface, the evident experimental result is that mainly the two C3 carbohydrates are produced from glycerol. On Merck TiO_2 almost no change is observed with addition of fluorides, while on P25 the production of formaldehyde and glycolaldehyde was strongly depressed. As fluorides impede the surface complexation on the surface Ti-OH site,

the formation of formaldehyde and glycolaldehyde is strictly connected with glycerol chemisorption.

When the surface is fluorinated, the surface complex (Ti(OR)(OH)) is no more allowed and only oxidative attack mediated by Ti(F)(O•) shallow surface hole traps is possible. In this case the two produced carbon-centered radicals evolve to dihydroxyacetone (C3) or glycerolaldehyde (C3) as in OH radical chemistry. The rates for glycerol degradation measured on fluorinated P25 [68, 105] (with most adsorption sites masked) are very similar to that on fluorinated and pristine Merck, except for a higher factor 4–5 that was ascribed to the different surface area of catalysts.

All the above results suggest that fluorination impedes surface complexation by substrates to be oxidized and renders the surface hole trap more shallows and resonant with valence band hole. The electron transfer will then follow the mechanism and energetics similar to that of free OH radicals.

4 Conclusions

The concepts of electron transfer *across* the interface and *at* the interface, together with the very nature of surface traps, are able to qualitatively (and in some case quantitatively [105]) explain the reactivity of electrons and holes produced by light absorption in semiconductors. The nature of surface traps depends on the crystalline phase and the specimen, as different surface hydroxyls are present with different complexing ability toward inorganic and organic species. The electron transfer *across* the interface is limited to few physisorbed species in some materials (e.g., P25) and is more common with others (e.g., anatase Merck). The reverse is true for electron transfer *at* the interface. The trap energy position, and consequently the trapping timescale and the overall process rate, depends on the photocatalyst, the substrate, and its concentration. Experiments with defined substrates under arbitrary chosen concentrations can be misleading. The functional dependence of the experimental response (IR, EPR, luminescence, overall rate... also time resolved) from the surface coverage of the substrate and other competitive complexing species is the suggested recipe to better understand the catalytic sites at the TiO_2 surface.

Acknowledgements The University of Torino support by Ricerca Locale 2012 is kindly acknowledged.

References

1. Watanabe M, Hayashi T (2005) J Lumin 112:88–91
2. Berger T, Sterrer M, Diwald O, Knözinger E, Panayotov D, Thompson TL, Yates JT Jr (2005) J Phys Chem B 109:6061–6068

3. Emeline AV, Frolov AV, Ryabchuk VK, Serpone N (2003) J Phys Chem B 107:7109–7119
4. Fu Y, Cao WH (2006) J Appl Phys 100:084324
5. Planelles J, Movilla JL (2006) Phys Rev B 73:235350
6. Tamaki Y, Furube A, Murai M, Hara K, Katoh R, Tachiya M (2007) Phys Chem Chem Phys 9:1453–1460
7. Rabani J, Yamashita K, Ushida K, Stark J, Kira A (1998) J Phys Chem B 102:1689–1695
8. Katoh R, Murai M, Furbe A (2008) Chem Phys Lett 461:238–241
9. Tamaki Y, Hara K, Katoh R, Tachiya M, Furube A (2009) J Phys Chem C 113:11741–11746
10. Bahnemann DW, Hilgendorff M, Memming R (1997) J Phys Chem B 101:4265–4275
11. Corrent S, Cosa G, Scaiano JC, Galletero MS, Alvaro M, Garcia H (2001) Chem Mater 13:715–722
12. Szczepankiewicz SH, Moss JA, Hoffmann MR (2002) J Phys Chem B 106:2922–2927
13. Peiro AM, Colombo C, Doyle G, Nelson J, Mills A, Durrant JR (2006) J Phys Chem B 110:23255–23263
14. Ikeda S, Sugiyama N, Muratami S, Kominami H, Kera Y, Noguchi H, Uosaki K, Torimoto T, Ohtani B (2003) Phys Chem Chem Phys 5:778–783
15. Szczepankiewicz SH, Colussi AJ, Hoffmann MR (2000) J Phys Chem B 104:9842–9850
16. Henderson MA (2011) Surf Sci Rep 66:185–297
17. Warren DS, Mcquillan AJ (2004) J Phys Chem B 108:19373–19379
18. Diebold U (2003) Surf Sci Rep 48:53–229
19. Micic OI, Zhang YN, Cromack KR, Trifunac AD, Thurnauer MC (1993) J Phys Chem 97:7277–7283
20. Serpone N, Lawless D, Khairutdinov R, Pelizzetti E (1995) J Phys Chem 99:16655–16661
21. Ke SC, Wang TC, Wong MS, Gopal NO (2006) J Phys Chem B 110:11628–11634
22. Deskins NA, Dupuis M (2009) J Phys Chem C 113:346–358
23. Hurum D C, Gray K A, Rajh T, Thurnauer M C (2005) J Phys Chem B 109:977–980, erratum 5388
24. Dimitrijevic NM, Saponjic ZV, Rabatic BM, Poluektov OG, Rajh T (2007) J Phys Chem C 111:14597–14601
25. Berger T, Sterrer M, Diwald O, Knozinger E, Panayotov D, Thompson TL, Yates JT Jr (2005) J Phys Chem B 109:6061–6068
26. Yoshihara T, Tamaki Y, Furube A, Murai M, Hara K, Katoh R (2007) Chem Phys Lett 438:268–273
27. Tamaki Y, Furube A, Murai M, Hara K, Katoh R, Tachiya M (2006) J Am Chem Soc 128:416–417
28. Minero C (1999) Catal Today 54:205–216
29. Minero C, Vione D (2006) Appl Catal B Environ 67:257–269
30. Gao R, Safrany A, Rabani J (2003) Radiat Phys Chem 67:25–39
31. Berger T, Lana-Villarreal T, Monllor-Satoca D, Gómez R (2007) J Phys Chem C 111:9936–9942
32. Minella M, Faga MG, Maurino V, Minero C, Pelizzetti E, Cosuccia S, Martra G (2010) Langmuir 26:2521–2527
33. Primet M, Pichat P, Mathieu M-V (1971) J Phys Chem 75:1216–1220; 75:1221–1226
34. Connor PA, Dobson KD, McQuillan AJ (1999) Langmuir 15:2402–2408
35. Hiemstra T, Van Riemsdijk WH (2006) J Colloid Interface Sci 301:1–18
36. Machesky ML, Wesolowski DJ, Palmer DA, Ridley MK (2001) J Colloid Interface Sci 239:314–327
37. Fitts JP, Machesky ML, Wesolowski DJ, Shang XM, Kubicki JD, Flynn GW, Heinz TF, Eisenthal KB (2005) Chem Phys Lett 411:399–403
38. Ambrus Z, Mogyorósi K, Szalai A, Alapi T, Demeter K, Dombi A, Sipos P (2008) Appl Catal A Gen 340:153–161
39. Gomathi DL, Narasimha MB, Girish KS (2009) Chemosphere 76:1163–1166
40. Vargas R, Núñez O (2009) J Mol Catal A Chem 300:65–71

41. Fujishima A, Zhang X, Tryk DA (2008) Surf Sci Rep 63:515–582
42. Kimmel GA, Petrik NG (2008) Phys Rev Lett 100:196102
43. Imanishi A, Okamura T, Ohashi N, Nakamura R, Nakato Y (2007) J Am Chem Soc 129:11569–11578
44. Cornu CJG, Colussi AJ, Hoffmann MR (2003) J Phys Chem B 107:3156–3160
45. Liang H-C, Li X-Z, Yang Y-H, Sze K-H, (2008) Chemosphere 73:805–812
46. López-Muñoz MJ, Aguado J, Arencibia A, Pascual R (2011) Appl Catal B Environ 104:220–228
47. Ohno T, Sarukawa K, Matsumura M (2002) J Chem 26:1167–1170
48. Petrik NG, Zhang Z, Du Y, Dohnálek Z, Lyubinetsky I, Kimmel GA (2009) J Phys Chem C 113:12407–12411
49. Henderson MA, Epling WS, Peden CHF, Perkins CL (2003) J Phys Chem B 107:534–545
50. Nakamura R, Imanishi A, Murakoshi K, Nakato Y (2003) J Am Chem Soc 125:7443–7450
51. Maurino V, Minero C, Mariella G, Pelizzetti E (2005) Chem Commun (20):2627–2629
52. Haick H, Paz Y (2003) ChemPhysChem 4:617–620
53. Tachikawa T, Majima T (2010) Chem Soc Rev 39:4802–4819
54. Thiebaud J, Thévenet F, Fittschen C (2010) J Phys Chem C 114:3082–3088
55. Anpo M, Shima T, Kubokawa Y (1985) Chem Lett (12):1799–1805
56. Henderson MA (2002) Surf Sci Rep 46:1–308
57. Di Valentin C, Pacchioni G, Selloni A (2006) Phys Rev Lett 97:166803
58. Nosaka Y, Komori S, Yawata K, Hirakawa T, Nosaka YA (2003) Phys Chem Chem Phys 5:4731–4739
59. Howe RF, Graetzel M (1987) J Phys Chem 91:3906–3911
60. Micic OI, Zhang Y, Cromack KR, Trifunac AD, Thurnauer MC (1993) J Phys Chem 97:13284–13289
61. Lawless D, Sermone N, Meisel D (1991) J Phys Chem 95:5166–5170
62. Minero C, Catozzo F, Pelizzetti E (1992) Langmuir 8:481–486
63. Minero C, Mariella G, Maurino V, Pelizzetti E (2000) Langmuir 16:2632–2641
64. Minero C, Mariella G, Maurino V, Pelizzetti E (2000) Langmuir 16:8964–8972
65. Pang CL, Lindsay R, Thornton G (2008) Chem Soc Rev 37:2328–2353
66. Byrne JA, Eggins BR, Linquette-Mailley S, Dunlop PSM (1998) Analyst 123:2007–2012
67. Berger T, Rodes A, Gómez R (2010) Phys Chem Chem Phys 12:10503–10511
68. Bedini A, Maurino V, Minella M, Minero C, Rubertelli F (2008) J Adv Oxid Technol 11:184–192
69. Wen B, Li Y, Chen C, Ma W, Zhao J (2010) Chem Eur J 16:11859–11866
70. Nelson BP, Candal R, Corn RM, Anderson MA (2000) Langmuir 16:6094–6101
71. Kormann C, Bahnemann DW, Hoffmann MR (1991) Environ Sci Technol 25:494–500
72. Murakami N, Chiyoya T, Tsubota T, Ohno T (2008) Appl Catal A General 348:148–152
73. Liu L, Zhao C, Li Y (2012) J Phys Chem C 116:7904–7912
74. Franch MI, Ayllon JA, Peral J, Domenech X (2005) Catal Today 101:245–252
75. Wu JCS, Cheng Y-T (2006) J Catal 237:393–404
76. Chen CC, Li XZ, Ma WH, Zhao JC, Hidaka H, Serpone N (2002) J Phys Chem B 106:318–324
77. Pelet S, Moser JE, Grätzel M (2000) J Phys Chem B 104:1791–1795
78. Minero C, Maurino V, Pelizzetti E (1997) Mar Chem 58:361–372
79. Franch MI, Peral J, Domenech X, Ayllon JA (2005) Chem Commun 14:1851–1853
80. Maurino V, Minero C, Pelizzetti E, Mariella G, Arbezzano A, Rubertelli F (2007) Res Chem Intermed 33:319–332
81. Connor PA, McQuillan AJ (1999) Langmuir 15:2916–2921
82. Kataoka S, Gurau MC, Albertorio F, Holden MA, Lim S-M, Lim S-M, Yang RD, Cremer PS (2004) Langmuir 20:1662–1666
83. Stone AT (1996) Environ Sci Technol 30:1604–1613

84. Yang HG, Sun CH, Qiao SZ, Zou J, Liu G, Campbell Smith S, Cheng HM, Lu GQ (2008) Nature 453:638–642
85. Park H, Choi WJ (2004) J Phys Chem B 108:4086–4093
86. Vohra MS, Kim S, Choi WJ (2003) J Photochem Photobiol A 160:55–60
87. Vione D, Minero C, Maurino V, Carlotti ME, Picatonotto T, Pelizzetti E (2005) Appl Catal B Environ 58:81–90
88. Mrowetz M, Selli E (2006) J Chem 30:108–114
89. Park H, Choi W (2005) Catal Today 101:291–297
90. Chiang K, Amal R, Tran TJ (2003) Mol Catal 193:285–297
91. Lee J, Choi W, Yoon J (2005) Environ Sci Technol 39:6800–6807
92. Yu J, Zhang J (2010) Dalton Trans 39:5860–5867
93. Dozzi MV, Schiavello GL, Selli E (2010) J Adv Oxid Technol 13:305–312
94. Chen Y, Chen F, Zhang J (2009) Appl Surf Sci 255:6290–6296
95. Chen KT, Lu CS, Chang TH, Lai YY, Chang TH, Wu CW, Chen CCJ (2010) Hazard Mater 174:598–609
96. Lv K, Li X, Deng K, Sun J, Li X, Li M (2010) Appl Catal B Environ 95:383–392
97. Mrowetz M, Selli E (2005) Phys Chem Chem Phys 7:1100–1102
98. Park JS, Choi W (2004) Langmuir 20:11523–11527
99. Lv K, Xu Y (2006) J Phys Chem B 110:6204–6212
100. Monllor-Satoca D, Gomez R, Gonzalez-Hidalgo M, Salvador P (2007) Catal Today 129:247–255
101. Xu Y, Lv K, Xiong Z, Leng W, Du W, Liu D, Xue X (2007) J Phys Chem C 111:19024–19032
102. Monllor-Satoca D, Gomez R (2008) J Phys Chem C 112:139–147
103. Monllor-Satoca D, Lana-Villarreal T, Gómez R (2011) Langmuir 27:15312–15321
104. Montoya JF, Salvador P (2010) Appl Catal B Environ 94:97–107
105. Minero C, Bedini A, Maurino V (2012) Appl Catal B Environ 128:135–143

http://www.springer.com/978-3-662-46794-7

Environmental Photochemistry Part III
Bahnemann, D.W.; Robertson, P.K.J. (Eds.)
2015, XIV, 346 p. 149 illus., 70 illus. in color., Hardcover
ISBN: 978-3-662-46794-7